Enhanced Genetic Disorder based Chromosomal Abnormal detection Using Deep Vectorized Scaling Neural Network Approach

P Srinivasan[1*] and R. S Sabeenian[2†]

[1*]Department of Electronics and Communication Engineering Sona College of Technology, Salem-5, Tamil Nadu, India.
[2]Department of Electronics and Communication Engineering Sona College of Technology, Salem-5, Tamil Nadu, India.

*Corresponding author(s). E-mail(s): srinivasan2024p@gmail.com;
Contributing authors: Sabeenian@yahoo.com;
†These authors contributed equally to this work.

Abstract

Chromosomal anomaly causes the development of fetus growth defect, which is identified in ultrasound images by analyzing Down syndrome samples. Researchers have designed different methods for analyzing chromosomal data, employing soft computing optimized with an ML approach and examining micro Down syndrome samples. Still, detecting genetic disorders in the fetus is difficult. However, it is necessary to identify variation differences in genetic-based chromosomes accurately. Since feature variants project similar dimensional structures, the resulting recognition errors may prevent accurate anomaly detection. To address these issues, this research develops an Invariant Structural Cascade Segmentation (ISCS) based on a Deep Vectorized Scaling Neural Network (DVSNN) technique to automatically detect genetic-based chromosome defects from ultrasound images for early diagnosis. Initially, the Fetus Ultrasound image dataset is gathered, and Adaptive Median Filter (AMF) are used to obtain a noise-free fetus image. After preprocessing the image, the Invariant structural cascade segmentation (ISCS) method is employed to segment it. This method determines the features like texture, color, and pixel intensity. Subsequently, the Angular Vector Projection (AVP) technique is applied to analyze the structural variance of cells. Afterward, the Histogram Color Equalizer (HCE) approach is used to choose the irregularity cells using K-counts and feature weight. Based on feature weight, the proposed DVSNN algorithm is used to categorize the risk of genetic disorders based on chromosomal abnormality. Our approval showed empowering

results while coordinating chromosomes with noticeable and undetectable banding designs. Therefore, the proposed method is helpful in solving concerns related to genetic-based chromosome image analysis, such as segmentation and cytogenetic classification. This effectively identifies chromosome abnormalities in micro image cells to detect patients at risk. Compared to traditional approaches, the proposed method improves classification accuracy, precision, and recall rate.

Keywords: Chromosomal, anomaly, syndrome samples, micro image, cytogenetic, genetics disorder, feature weight, structural abnormalities, patients, classification.

1 Introduction

Global studies indicate that approximately 8% of people suffer from genetic syndromes, and most genetic diagnoses are usually constructed after childbirth [1]. Genetic diseases account for approximately 80% of rare conditions and are caused by genetic changeovers. They can cause disability, impairment, and intellectual disability in patients, and in severe cases, even death in kids[2] . Chromosomal abnormal detection is a crucial aspect of genetic testing that allows healthcare professionals to identify any irregularities or abnormalities in an individual's chromosomes. These abnormalities can have a wide range of consequences, from mild physical or developmental issues to more severe genetic disorders. By detecting these abnormalities early on, medical professionals can provide appropriate treatment and support to patients and their families.

Identification of genetic diseases associated with pregnancy is of tremendous significance in the analysis and treatment of genetic illnesses during pregnancy [3]. Fetal abnormalities refer to abnormal fetal development during pregnancy, while congenital disabilities and birth defects are closely related terms. Fetal malformations have been commonly observed in developed countries for decades. Out of 1,000 pregnant women suffer from fetal malformations. Ultrasound medical images allow for easy fetal identification and calculating of fetal parameters using segmentation techniques.

Anomaly detection is an urgent and important task for various applications, but more adequate methods are needed to meet the requirements. The challenge in anomaly detection is distinguishing between various or unknown anomalies. Fetal imaging in high-risk pregnancies has been incorporated into regular and continuous monitoring of fetal parameters. These parameters detect fetal weight, growth status, gestational age, and possible abnormalities. Chromosomal aberrations were detected in 301 cases (14%) and were more common in multisystem malformation fetuses (29%) than isolated defects (2%).

Most fetuses with cytogenetic irregularities have outer or inside absconds that can relate to nitty gritty ultrasonography. Without much of a stretch, routine assessments can recognize many deformities, yet others require unique consideration. In this way,

before leading examinations assessing the job of ultrasound in evaluating for fetal chromosomal anomalies, it is essential to consider the sorts of irregularities related to every contortion and the various kinds of chromosomal abnormalities recognized by ultrasound. The phenotypic manifestation of fetal chromosomal abnormalities must be determined.

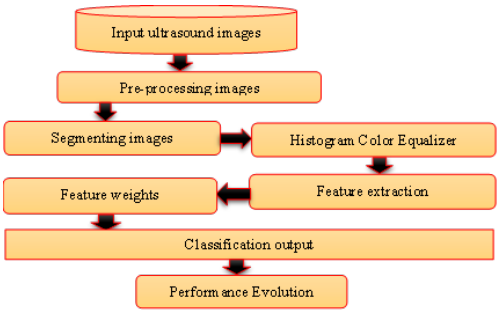

Fig. 1 Basic Flow diagram

Figure 1 demonstrates the basic work flow diagram of Chromosomal anomaly for the proposed approach, which includes steps of ultrasound fetal image Pre-Processing, Feature Extraction, classification output and validation performance analysis—classifying fetal ultrasound images as "normal" or "abnormal" based on the proposed classification performance evaluation using ultrasound images.

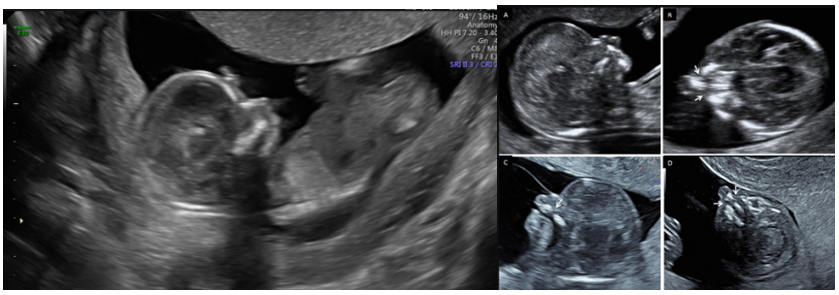

Fig. 2 Trisomy (13) Paatu Syndrome

Trisomy 13, also called Patau syndrome, is a genetic disorder characterized by an extra copy of genetic material on chromosome 13. This disorder can lead to a type of severe medical concerns, including severe intellectual disability and physical abnormalities. As shown in Figure 2, children born with trisomy 13 have heart defects, brain abnormalities, and other organ defects. Low-level lesions require highly

sensitive samples and robust noise handling, and detection is complicated because the proportion of abnormal cells varies between different tissues and developmental stages. To fill these research gap, this paper presents the AMF method adapts to the local statistics, to minimize noise effects, without blurring coarse structural definition. The ISCS approach provides cleaner segmentation masks leading to better quality and consistency of downstream texture, color and intensity analysis. AVP method provides the set of features with directional invariance and discriminating angular data useful in distinguishing between normal and abnormal chromosomal patterns. HCE approach identifies more stable and differentiating space of color features on the basis of which irregularities caused by chromosome abnormalities are specified more precisely. And lastly, the scaling data in vectors attribute of the DVSNN algorithm means that the network will be capable of dealing with multi-scale representation of data characteristics and transitioning to different magnitudes across characteristics categorical risk evaluation (e.g. low/medium/high risk) which integrates multiple modalities into a final diagnosis outcome.

1.1 Contribution of this paper

- To implement an adaptive media filter is used to ensure a noise-free image for accurate analysis.
- The ISCS method enabled the partitioning of microcells in the images, allowing for the identification of important features such as texture, pixel colour, and intensity.
- To design a proposed AVP method is utilized to detect variations in the structural components of cells, aiding in identifying abnormalities.
- The HCE approach selects abnormal cells based on K-counts and their feature weight, enhancing abnormality detection accuracy.
- The selected features and their weights were trained in a DVSNN to categorize the risk of genetic disorder based chromosomal abnormality, improving the efficiency and accuracy of the detection process.

1.2 Outline of the research

The introduction briefly outlines the importance of detecting chromosomal abnormalities in section 1. The literature survey then analyzes the merits and demerits of every approaches and identifies gaps in current approaches in section 2. Additionally, section 3 presents a detailed methodology on how DVSNN can be utilized for chromosomal abnormality detection, covering data preprocessing, segmentation, and prediction processes. Section 4 delves into the results, showcasing outcomes achieved through the DVSNN method and comparing its performance to other techniques. Lastly, the conclusion summarizes key findings and discusses the implications of the proposed methodology for future research and clinical practice.

2 Related work

Chromosomal varieties are an essential instrument for guaranteeing the endurance of a sound infant and finding and expecting Turner's condition utilizing the outfit learning technique using facial images. The typical clinical chromosomal problem is Turner's condition, additionally called inborn uterine hypoplasia disorder. With the guide of cytogenetic analytic outcomes, the demonstrative exactness of paediatricians is sufficient [4]. The mind-boggling data and weighty responsibility of karyotype imaging are the primary difficulties of clinical determination[5] . Propose an original Various-Net technique that utilizes profound convolutional organizations to characterize chromosome type and extremity while accelerating diagnosis. This scheme consists of a Global network (G-Net) and a local Scale network (L-Net) [6].

A Deep learning based Convolutional Neural Network (CNN) method is proposed for programmed chromosome arrangement. The suggested approach was developed and tested on a dataset consisting of 10304 chromosome images and additionally tested on a dataset comprised of 4830 chromosomes [7]. Creating computerized frameworks for chromosome characterization and anomaly discovery in leukaemia is fundamental in cytogenetics. Such a framework can be successfully used to find acquired illnesses and, with the assistance of karyotyping, can be utilized for remedial assessment strategies, guess expectation and ensuing treatment. This is conceivable because mathematical and underlying chromosomal anomalies are often typical for leukaemia [8].

Specialists use chromosome examination for early recognition, anticipation, and assessment of treatment for hereditary problems like leukaemia and Down disorder. The analysis is completed utilizing karyotype. Karyotype investigation is a burdensome assignment [9]. Pre-birth evaluation for chromosomal irregularities is an essential instrument for guaranteeing the sound endurance of infants. Karyotype image examination has complex data and high responsibility, which is a significant issue in clinical findings [10]. Pre-birth evaluation for chromosomal irregularities is a powerful instrument for guaranteeing the solid endurance of infants. Scientific data of karyotype images need to be more precise and complex, which is a significant issue in clinical diagnosis [11].

Karyotyping is working seriously, space mastery and experience-concentrated, and tedious. Computerizing, the most common way of karyotyping is a significant and welcome test. This review zeroed in on the characterization of chromosomes into 23 classifications, a stage towards completely robotized karyotyping [12]. Pre-birth evaluation for chromosomal irregularities is an effective method for guaranteeing the endurance of a sound infant. Karyotype image examination data is perplexing, responsibility serious, and an actual test in clinical findings.

The chromosomal arrangement is essential to karyotyping in diagnosing anomalies. To accelerate the conclusion, we propose another technique called profound Organization. It simultaneously utilizes a deep convolutional organization to describe chromosome type and extremity [13] simultaneously. Improvement of a robotized answer for the

quick, high-throughput, mechanized discovery of chromosomal aberrations (CAs) in word-related well-being checking of enormous scope radiation labourers. We approved the precision of another evaluation framework in light of mechanized loose bowels chromosome (DIC) filtering and examination [14]. There is an earnest need to lay out a computerized answer for fast, high-throughput mechanized location of chromosomal abnormalities (CA) in word-related well-being checking of enormous scope radiation labourers [15].

Detailed computerized image examination of strange tiny designs depends on top-notch images with a negligible rate of bogus up-sides (FPs) and undesirable articles in the images. Cytogenetic biodosimetry recognizes bicentric chromosomes (DCs) presented to ionizing radiation and decides the radiation got given the DC recurrence [16]. This strategy utilizes grouping and watermarking calculations to portion the crude chromosome image and distinguish individual chromosomes [17]. Chromosome examination is a crucial undertaking in the cytogenetics research facility, which permits us to decide the presence or nonattendance of cytogenetic irregularities. Karyotyping is a standard strategy for chromosome examination that groups metaphase images into 24 chromosome classes [18].

Chromosome sorting and karyotype analysis are essential steps in diagnosing genetic diseases. Most cytogenetic laboratories have developed various computer-aided systems, such as deep learning, to automate this problematic task [19]. Unfortunately, chromosomes are often duplicated, so it is necessary to identify and distinguish duplicate chromosomes. A rapid and automated fractionation solution enables cost-effective drug quantification [20].
Division requires the improvement of this framework to recognize and separate individual chromosomes. A significant test in chromosome division is isolating covering chromosomes. Deep Convolutional Neural Networks (DCNNs) have been broadly utilized in the clinical field, particularly in U-Net [21]. A solid independent framework for ordering human chromosomes will set aside time and cash and diminish blunders brought about by the absence of mastery. Human cells include 23 sets of chromosomes, 22 sets of autosomes, and 1 set of chromosomes. Then, they face the multi-class clustering task, which is a complex situation for any feature description [22].

Chromosomal order assumes a significant part in determining a karyotype. An average human chromosome has 46 chromosomes. Karyotyping is a powerful clinical technique for detecting congenital infections and diseases. As manual karyotyping is concentrated and tedious, creating robotized PC-supported frameworks is progressively significant [23]. Karyotyping at present requires a great deal of manual work, space skill, and experience and is tedious. Robotizing the method involved with karyotyping is a significant and everyday task [24].
The outcome of most classical classification methods depends on exact chromosome division. Even with long periods of examination around here, the exact division and order of cell bunches and pathology, if any, stays a test [25]. Because of the complex morphological elements of chromosomal bunches, chromosomal occasion division is

the main deterrent for robotized karyotyping, which restricts the high dependability of karyotyping to talented clinical agents [26].

The mind-boggling data and touchy capacities of karyotyping imaging are significant tests in clinical conclusion [27]. Mechanized chromosome sequencing has been focused on as of late as additional patient examples are exposed to clinical trials like bone marrow biopsies. With the progression of artificial consciousness, CNN has shown better performance in image recognition [28]. To mitigate extreme impeding issues, we present a different format block branch notwithstanding the customary recognition branch. It utilizes the calculation data of the chromosomes to extricate the particular embeddings for each suggestion [29]. Karyotyping is the most established research facility strategy for the manual division of chromosomes to distinguish chromosomal irregularities. A survey of karyotyping and past audits of other ordered groupings showed that this characterization could be more precise [30]. Karyotypes were acquired by examining the meta-diffuse chromosome images. Chromosome images in meta-propagation frequently contain issues connected with chromosome duplication and linkage. Isolation and isolation of connecting chromosomes remain an open issue [31].

Atomic testing is becoming progressively significant in the analysis of malignant growth. Designated next-generation sequencing (NGS) is a generally acknowledged technique, yet the recognition of underlying variations (SV) by designated NGS stays a test [32]. DCA is considered the "best quality level" for surveying consumed radiation. This is because bicentric chromosome development is well-defined for ionizing radiation openness and has a shallow base recurrence in unexposed people. Even so, the exhibition of DCA for organic dosimetry is relentless and tedious, making its utilization for radiation/atomic mass setbacks illogical [33].

Numerous applications, such as the precise diagnosis and grading of numerous malignancies, the differential diagnosis of autoimmune illnesses, and the investigation of physiological processes, are based on automated system analysis. The design and analysis of biological imaging systems have garnered significant attention in recent times owing to their distinct features and challenges [34]. The quantity of dead cells in tumour tissue is a significant factor in GBM brain tumors, hence early identification of Glioblastoma (GBM) tumor malignancy is crucial [35]. It takes the fulfilment of both of these requirements for glaucoma to develop. The Otsu threshold segmentation approach was utilized to obtain the diameters of the vertical optic cup and optic disc. The vertical diameter of the disk is divided by the vertical diameter of the cup to determine the cup-to-disk ratio [36]. The gold standard used by ophthalmologists to diagnose glaucoma is the ISTN. Creating and putting into practice a health monitoring architecture utilizing an Arduino UNO microcontroller unit with WiFi, a wireless biomedical parameter monitoring system, and a variety of biomedical sensors [37]. The device takes physiological parameters including heart rate and vital signs [38]. Essentially, the use of artificial intelligence in computer-assisted tomography is becoming more and more significant in intelligent healthcare monitoring systems. Because of security and privacy considerations, analyzing computed tomography

information has become a difficult procedure [39].

Current techniques input deep learning networks photos of the eyes, which may lead to incorrect iris features and undoubtedly lower accuracy. A deep learning neural network model called AlexNet uses preprocessed, precise iris boundaries as input for categorization [40]. Compared with current biometric technology, it offers several advantages. The wrist nerve, the palmar nerve, the finger nerve, and the frontal nerve make up the hand's nervous system [41]. Moles are present in every part of the human body and are utilized for identification. The growth of moles can result in cancer and melanoma. Cancer and eyesight loss can be avoided with early detection and development [42]. An individual's life expectancy can be increased by early detection of melanoma, although more analytical advancements are needed. The limit of abnormal skin damage is thought to be a crucial clinical component in the early diagnosis of melanoma [43]. Radiologists and other clinical professionals are very interested in magnetic resonance imaging (MR) imaging; yet, it is a laborious and time-consuming process, with accuracy solely dependent on experience. Thus, the use of computer-assisted technologies is required to get over these constraints [44]. Table 1 describes the summary of chromosomal abnormal detection based on ML and DL.

Table 1 Summary of chromosomal abnormal detection

Ref	Author (year)	Dataset used	Methods	Findings
[45]	Saranya Sekar et al. (2025)	Chromosomal images	Adaptive Residual DenseNet (ARDNet) and RU-ASBO	To achieve adequate performance for genetic disorder detection.
[46]	Tabassum, S. et al. (2025)	Chromosomal images	Autoencoder with CNN	Accurately find the neurodegenerative disorders.
[47]	Nimitha, N et al. (2025)	Chromosome images	Visual Geometric Transformer-based Mantis Search (VGT-MS)	It reduces computational overhead with enhanced abnormal detection accuracy.
[48]	C.-E. Kuo et al. (2025)	Metaphase cell images	ChromosomesNet	This method attained high accuracy for chromosome detection.
[49]	Mohammed El et al. (2023)	Inversion inv(3)	CNN with Siamese architecture	The offered method finds the structural chromosomal abnormalities.

2.1 Limitation of this work

- Existing Approaches using manual karyotyping are complicated, time-consuming and error-prone.
- Manually examining the images and determining the diagnosis based on the number, size, shape, and relationships of the various image segments is time-consuming.

- The previous method didn't concentrate on segmentation and image quality enhancement.
- The chromosomal abnormal detection is a challenging problem because of the wide variability due to many factors, including maternal obesity, abdominal scarring, amniotic fluid volume, and extensive container ligatures.
- Not efficient for detecting fetal abilities and identifying them.
- The traditional methods produce less accuracy performance.

3 Materials and Method

Genetic-based chromosome analysis based on DL is a fundamental task in genomics laboratories. It helps the geneticists to detect the presence or absence of abnormalities. Genetic Information from 381 pregnant ladies to inspect the proposed model, referring to an underground evaluating reference research facility for early pregnancy screening, and fetal ultrasound images at 11-13 weeks old were collected. The proposed model in this work uses an ISCS based on DVSNN techniques for genetic-based chromosome abnormal detection. It helps to classify the numerical anomalies in a dataset collected from non-overlapping metaphase images.

Figure 3 describes the first input of the Fetus Chromosome abnormality Image

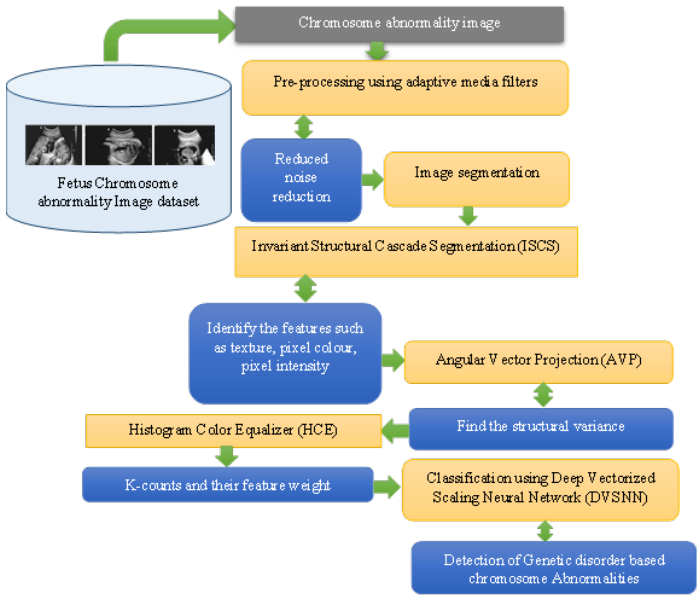

Fig. 3 Proposed block diagram

dataset from the Kaggle repository; then, we enter the pre-processing stage for reducing noise based on the adaptive median filter. The second stage is segmentation, which separates ISCS-based features (size, texture, pixel color, and intensity) and detects

the structural contrast used in AVP to extract features to improve the quality and color of the extracted image based on HCE. Find the k-counts of the feature weights. Finally, the DVSNN was used to characterize the risk of chromosomal abnormalities.

3.1 Fetus Chromosome Abnormality Ultrasound Image Dataset

The name of the gathered dataset is Ultrasound Fetus Dataset [50]. The collected image is split into training (70%), testing (15%), and training (15%). A computerized solution for chromosomal Abnormality identification and chromosomal Abnormality classification Ultrasound medical imaging tackle can quickly identify and quantify fetal parameters using segmentation techniques. Abnormal conditions of the fetus can be detected in time so that pregnant women can take necessary measures.
We collected 300 metaphase images containing normal and abnormal measurement cases with a resolution of 910 × 910 pixels and jpg file format. Selected images are presented in detail, and several curves are to have different band targets between 550 and 650. This dataset is utilized in the single-chromosome identification, grouping, and abnormality location stages. A single chromosome is produced by the process of detection. A total of 6807 chromosomes of 31×62, 51×67, 100×200, 69×82 and 43×62 were isolated in Figure 4.

Fig. 4 sample of chromosome images

3.2 Adaptive Median Filter (AMF) for Image Pre-processing

The proposed AMF method is utilized in the pre-processing stage of the Fetus Ultrasound image dataset. This filter is effective in reducing noise and enhancing the quality of images, especially in scenarios where the data is limited or of lower quality. By applying this filter, the dataset is prepared for further analysis and feature extraction, even when dealing with suboptimal image quality. The AMF works by analyzing the pixel values in a sliding window and determining the most suitable value for each pixel based on the neighbourhood. This proposed approach makes it particularly useful for images with varying levels of noise and distortion, as it can adjust its filtering parameters according to the local characteristics of the image.
A_{min} = Minimum values of image pixel in l_{ab}
A_{max} = Maximizing the image field in l_{ab}

A_{med} = Median values of the image field in l_{ab}
A_{ab} = image values pixel in coordination (a, b)
I_{max} = Maximum possible value for l_{ab}
The Adaptive median filter is used to smoothen the image noises and enhance the image contrast level.

$$\text{local mean(a,b)} = \mu = \frac{1}{N^2} \sum_{a=-\frac{N}{2}}^{\frac{N}{2}} \sum_{a'=-\frac{N}{2}} a(a + a', b + b') \tag{1}$$

$$\text{Local variance (a,b)} = \sigma^2 = \left[\frac{1}{N^2} \sum_{a=-\frac{N}{2}}^{\frac{N}{2}} \sum_{a'=-\frac{N}{2}}^{\frac{N}{2}} a(a + a', b + b') \right] - \mu^2 \tag{2}$$

Where a and b are images, each region has a size of NxN pixels. The region standard deviation is the square value of the variance.

$$I(a, b) = \left[1 - \frac{\sigma_x^2}{\sigma_y^2} \right] A(a, b) + \frac{\sigma_x^2}{\sigma_y^2} \mu_1 \tag{3}$$

o_x^2-noise variance, If the noise variance dominates the local variance, the local mean will be given. Adaptive filters are primarily based on local pixel statistics, i.e. the mean and variance of the pixels in the current neighbourhood. The local average is the average of the pixel concentrations in that region. The regional variance is computed based on the current region's pixels.

3.3 Invariant Structural Cascade Segmentation (ISCS)

Ultrasound medical images use segmentation techniques to identify beginnings and quantify fetal parameters quickly. Abnormal conditions of the fetus can be detected in time so that pregnant women can take necessary measures.

$$S_{Str}^{*} = \int_0^1 S_{str}(C(s)) = \int_0^1 [l_{int}(C(s) + l_{ext}(C(s))] \tag{4}$$

$$S_{int}\big(C(s)\big) = \left[\frac{1}{2} \alpha(s) |C(s)|^2 + \frac{1}{2} \alpha(s) |C_s(s)|^2 \right] \tag{5}$$

$$S_{ext}\big(C(s)\big) = -\gamma |\nabla \big[I_\sigma(a, b) * l(a, b) \big]|^2 \tag{6}$$

Where $I(a, b)$ - image positions, $S_{int}(C(s))$ - internal image points, and $S_{ext}(C(s))$ - external positions. An Invariant Structural Cascade Segmentation (ISCS) is proposed using highly inequality and feature-correlated data.

Image segmentation is often evaluated using pixel-level class labels, which addresses both limitations. Using ultrasound fetus images, ISCS is used to analysis the features (size, texture, pixel color, and pixel intensity). The loss function achieves the segmentation of ultrasound images. This method combines the elements segmented ISCS with the corresponding layer. Pick X (Max_False Positive rate per layer) and Y

(Min_False Positive (FP) acceptable Layers).

// T is Positive image samples, F-Negative image samples

$X_{Overall} is the Targeted FP range$

$X_0 = 1 and Y_0 = 1 do$

$while X_0 > X_{0verall}(X_i overall FP ratex)$

x + +(Layers increasing by 1)

$\mathrm{Xi} = 0; \mathrm{F_{x-1}}$(Xi : Negative samples of x)

While $\mathrm{Xi} > \mathrm{F} * \mathrm{F_{x-1}}$:

X++(Check next features samples).

Does not meet the integration criteria

$$\mathbf{C_s} = \frac{\iint \mathrm{l(a-b)l(b)q(a)V_i}(\varphi(\mathrm{b}))\mathrm{s_a s_b}}{\iint \mathrm{l(a-b)q^2(a)V_i}(\varphi(\mathrm{b}))\mathrm{s_a s_b}} \tag{7}$$

$$\sigma_{\mathrm{i}}^2 = \frac{\iint \mathrm{l(a-b)l(b)q(a)V_i}(\varphi(\mathrm{b}))^2\mathrm{s_a s_b}}{\iint \mathrm{l(a-b)V_i}(\varphi(\mathrm{b}))\mathrm{s_a s_b}} \tag{8}$$

Update the image features level using FP samples.

Segmented features→ using ISCS for Structural features

End while

For φ is variation image values, it can be shown parameters C_s, σ_i^2, q that estimate the feature values, weighted segment features of Fetus chromosome images based on the Invariant Structural Cascade Segmentation (ISCS).

3.3.1 Angular Vector Projection (AVP)

Fetus images represent information projections from different depths with angular. Due to the non-uniform signal scale, it is difficult to determine the depth direction from these projections. AVP gave the best results on linear chromosomes. For both linear chromosomes, the projected vectors were more accurate in centromeric detection for structural variance.

$$\mathrm{C_{xy}^{(h)}} = \sum_{\mathrm{s=1}}^{\mathrm{x}} \sum_{\mathrm{r=0}}^{\mathrm{y}} \binom{\mathrm{x}}{\mathrm{s}} \binom{\mathrm{y}}{\mathrm{r}} \mathrm{C_{xs}^{(h)}} \mathrm{C_{x-s,y-r}^{(h)}} \tag{9}$$

$C_{xy}^{(h)}$ and $C_{xs}^{(h)}$ are the vectorized $(x + y)^{\mathrm{th}}$ projections of the observed image. This method provides relatively accurate results for highly curved chromosomes. In our analysis, a velocity of 0.029 ± 0.005 mm·s^{-1} is detected, which, although close to the detection limit, indicates a weak bias for the movement of the vector segments towards the chromosomes.

Figure 5 Examined the efficacy of projection based on Angular vector and reported wide variations in screening detection rates from 35% to 100%. However, this finding excludes the possibility that projection vectors grow through chromosomes or their periphery. This is because the Angular vector region images the chromosome moving away from the chromosome at a rate comparable to the growth rate of microtubules that provide the angular projection. Projection indexing for angular deviation using segmentation images,

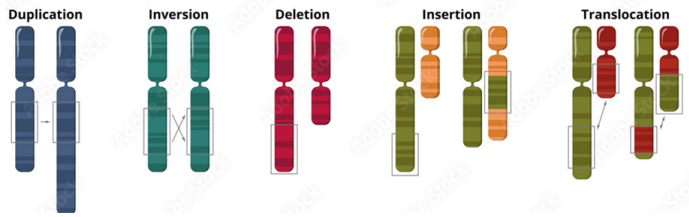

Fig. 5 Chromosome Abnormality Sample image for AVP

$$\Delta\phi_{\mathrm{x}} = \sqrt{\Delta \mathrm{a}_{\mathrm{x}}^2} + \sqrt{\Delta \mathrm{b}_{\mathrm{x}}^2}, \ldots, \mathrm{N} \tag{10}$$

$$\Delta \mathrm{a}_{\mathrm{x}} = \mathrm{a}_{\mathrm{x}} - \mathrm{a}_0, \tag{11}$$

$$\Delta \mathrm{b}_{\mathrm{x}} = \mathrm{b}_{\mathrm{x}} - \mathrm{b}_0, \tag{12}$$

Where $\varnothing_x$ represents the angular component, and b_x, a_x are the angles between the X and Y image axes. Different image descriptors, such as image moments and ranges, are invariant to interpretation, scaling, and rotation. Therefore, the motion blur of ultrasound images can be calculated through image interpretation.

3.4 Histogram Color Equalizer (HCE)

This method improves visual quality of digital images in large scenes and irregular lighting conditions ultrasound images. A histogram of a digital image with gray levels in the limit [0, L-1] is a discrete function,

$$\mathrm{S}(\mathrm{r_g}) = \mathrm{n_p}/\mathrm{n} \tag{13}$$

Here, r_g- intensity level in original raw images, n_p-number of the pixel in the grey scale images, n-total number of images, and g-grey level.

Here, r_g- intensity level in original raw images, n_p-number of the pixel in the grey scale images, n-total number of images, and g-grey level.

$$Greylevel \rightarrow \breve{\mathrm{g}} = \sum_{\mathrm{g}=0}^{\mathrm{H}-1} \mathrm{gP(g)} = \sum_{\mathrm{x}} \sum_{\mathrm{x}} \frac{\mathrm{H(h,w)}}{\mathrm{N}} \tag{14}$$

The total number of grey levels (Possible intensity values) N- the images using histogram matrix 256×1 to store the level (x) pixel. $n_x i$ is the number of pixels level r_g

$$\mathrm{His_{(a)}} = \mathrm{n_{xi}}, 0 \leq \mathrm{x} \leq \mathrm{i} \tag{15}$$

The pixel representation of projection includes an entity that supports "g" points corresponding to rows and columns with constant equalization variation from low-contrast pixels. This increases the degree of maturation, which is displayed as the

square root change in the sum of pixels

$$\sigma_{\mathrm{h}} = \sqrt{\sum_{\mathrm{h}=0}^{\mathrm{L}-1} (\mathrm{g} + \bar{\mathrm{g}})^2 * \mathrm{H}(\mathrm{g})} \tag{16}$$

To acquire a positive genetic image of a pixel, estimate the histogram gain by intensity levels within the occluded area. This is because it has a vector point of solid cover measurable.

$$\mathrm{C}(\mathrm{h}) = \sum_{\mathrm{n}=0}^{\mathrm{x}} \mathrm{H}(\mathrm{g}), \quad \mathrm{x} = 0, 1, \ldots, \mathrm{n} \tag{17}$$

$$\mathrm{C}_{\mathrm{h}}(\mathrm{H}') = \mathrm{C}_{\mathrm{h}}(\mathrm{R}(\mathrm{S}) = \mathrm{C}_{\mathrm{h}}(\mathrm{s})) \tag{18}$$

$$\mathrm{H}' = \mathrm{h}.\,(\max\{\mathrm{a}\} - \min\{\mathrm{a}\} + \min\{\mathrm{a}\}) \tag{19}$$

Where C increases the circulated function of image pixels, equalization is performed using the calculated image values on the greyscale images. S is the constant range of image points, a- used for normalizing the histogram ranges, and R- Levels the image range (0, 1).

Based on the color representation, the possibility of chromosome ultrasound fetus area is observed by the most significant individual scale as an eigenvector for further clarification.

Features weights Evaluation

The features weights Evaluation method separates color image regions based on the standard deviation of RGB. Assuming that the standard deviation S* is normalized between 0 and 1, the color image region for ultrasound chromosome abnormality images features weights calculation.

$$\mu(S^*) = \begin{cases} 0 \text{ if } 0 \leq \mathrm{S}^* > \mathrm{x} \\ 2\left(\dfrac{S^* - x}{y - x}\right)^2 \text{ if } \mathrm{x} \leq \mathrm{S}^* < \dfrac{\mathrm{x} + \mathrm{y}}{2} \\ 1 - 22\left(\dfrac{S^* - x}{y - x}\right)^2 \text{ if } \mathrm{x} \leq \mathrm{S}^* < \mathrm{y} \\ 1 \quad \text{if } \mathrm{y} \leq \mathrm{S}^* > 1 \end{cases} \tag{20}$$

Where x and y were given replace pixel values with x¡ y weights, an x,y=0.1

Each image pixel that belongs to a colour image area determines the importance of that pixel's hue and saturation components. Formally, it is denoted with values associated with each pixel.

$$\mathrm{w}_{\mathrm{P}}(\mathrm{x}, \mathrm{y}) \text{ and } \mathrm{w}_{\mathrm{q}}(\mathrm{x}, \mathrm{y}). \tag{21}$$

w_P And w_q are the weights of image intensity associated with the pixel (x, y). The weights of values are determined based on S^* values in that pixel.

$\mathrm{w}_{\mathrm{P}}(\mathrm{x}, \mathrm{y}) = \mu(\mathrm{S}^*(\mathrm{x}, \mathrm{y}))$ The weighted images intensity of histogram (H_1) are defined as,

$$\mathrm{w}_{\mathrm{P}}(\mathrm{x}, \mathrm{y}) = \mu(\mathrm{S}^*(\mathrm{x}, \mathrm{y})) \tag{22}$$

$$w_x(P) = \frac{\sum_{p,q} w_x(p,q)\delta(x(p,q)-1)}{\sum_{p,q} w_x(p,q)} \tag{23}$$

For each p=0,1,... $w_x(P)$, where δ the delta function of image values is, x stands for p and q. Get the updated histogram for each image in the database and store it in a 1xn size feature database, where n is the total number of images in the database.

3.5 Classification using Deep Vectorized Scaling Neural Network (DVSNN)

Chromosome classification by deep learning for Fetus abnormalities risk factors. It allows us to train and test images to predict chromosomal abnormalities. The proposed DVSNN, a scalable model, is required to select and manage features for a given genetic based chromosome dataset. Variations in the operational units are valid for a dynamic/auto-scalable approach. This method efficiently identifies genetic diseases or characterizes new chromosomal changes associated with genetic disorders in a reliable/scalable manner. A mean-vectorized scalable network for estimating abnormal risk scores of the kernel of continuous residual blocks before fully connected layers.

$N = \{X_h | h \in X\}$ In the activation set (N) included in the scaling area, 'X'is defined for evaluating the average risk factors (AS) = $\frac{\Sigma N_x}{|X_N|}$, and the Maximum weighted layer is defined as,

$$NX = Max(N_x) \tag{24}$$

The weighting information produced by each probability block indicates the role of location in the risk estimate. For fetal images, we calculated the image regions that could significantly impact the risk prediction of fetal abnormalities.

3.5.1 Detecting Individual Chromosome

Chromosomes can be identified by their number, size, centromere location, and banding pattern. The proposed method uses an object's state to identify the reality and associates all chromosomes with a bounding box.

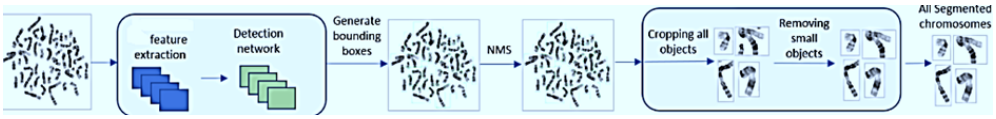

Fig. 6 Individual chromosome Detection

Object detection is solved as an evolution problem that spatially separates the bounding boxes and the corresponding class probabilities. Scaling utilizes highlights from the whole picture to foresee the limits of explicit locales. It has arrangement and limitation undertakings and can be prepared. The information picture is separated into cells in Figure 6. Each assumes a part in foreseeing class probabilities, jumping box areas, and box certainty scores (objective). During preparation, predefined bounding boxes of suitable shape and only incompletely established.

3.5.2 Classification stage

The following step is classification using DVSNN to categorize the genetic chromosomes correctly into their respective pairs. There are 23 pair's total, and the last pair forms the chromosome. To perform classification, the training DVSNN minimizes the number of parameters in the vectorized scalable network and reduces the sample size while maintaining better prediction accuracy.

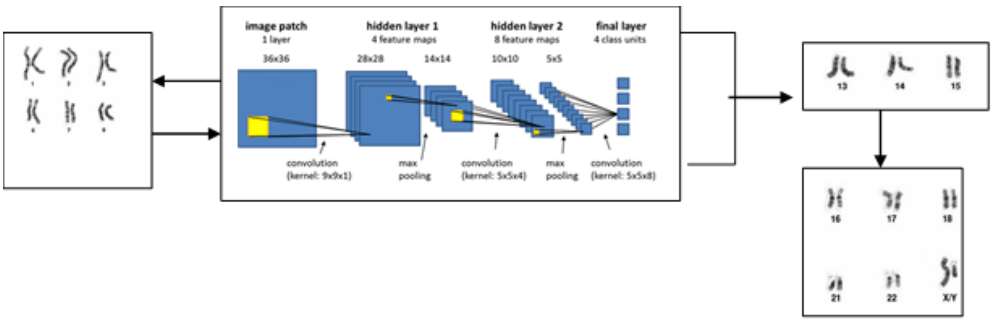

Fig. 7 Classification stage

Fully connected (FC) layers predict type and polarity, respectively—fully connected plots map feature vectors to 24-dimensional and 2-dimensional probability vectors. One of the important features of deep learning networks is their generalization ability to layers accurately. As shown in Figure 7, various regularization techniques have been proposed and proven to be effective in avoiding overfitting and making the model more stable.

Vectors Scalable Evaluation Scalable vectorized samples for Extricating highlights from input pictures of approval dataset.We calculate the 24 class features by averaging the feature vectors extracted from all samples in the same class.

$$\mathrm{F_v} = \gamma \frac{\sum_{\mathrm{x=1}}^{\mathrm{N}} \mathrm{f_v^x}}{\mathrm{N}} \quad \mathrm{v}\epsilon\{1, \mathrm{f_v}\}, \gamma\epsilon[1, 1.5] \tag{25}$$

Herein, F_v refers to feature scale vector, N denotes number of sample images, f_{vx} signifies the sample image feature vector and γ implies positive range among $1 \leq 1.5$.

$$\mathrm{H(x, y)} = \max\{\min_{\mathrm{A}\epsilon\mathrm{x}}\{||a, b||\}\} \tag{26}$$

Each metric that assesses the resemblance of two images is essential to improving classification accuracy. The Euclidean distance compares the correspondence of two images by comparing their element values (pixels). Categorize the input images by estimating the distinction between two input sets of the identical network classical and evaluate whether be appropriate to the equal class. Let us assume, f^c and f^d denotes the two attributes vectors.

$$c \in \mathbb{C} = \{c_1, c_2, ..., c_{\mathrm{fw}}\} \tag{27}$$

$$\mathrm{d} \in \mathrm{D} = \{\mathrm{d}_1, \mathrm{d}_2, ..., \mathrm{d}_{fw}\} \tag{28}$$

f_x^c-is the range of $f^t h$ element of feature vector f^c extracting the label vectors of the image dataset. f_x^d- is the image sample pixels values of the image set.

$$||\mathrm{a}, \mathrm{b}||_{\mathrm{e}} = \sqrt{\sum_{x=1}^{\mathrm{n}} (\mathrm{f}_{\mathrm{x}}^{\mathrm{c}} - \mathrm{f}_{\mathrm{x}}^{\mathrm{d}})^2} \tag{29}$$

$$||\mathrm{a}, \mathrm{b}||_{\mathrm{c}} = \mathrm{f}^c, \mathrm{f}^d /_{||f^c|| > ||f^d||} - \frac{\sum_{\mathrm{x}=1}^{n} \mathrm{f}^c \times \mathrm{f}^d}{\sqrt{\sum_{\mathrm{x}=1}^{n} (\mathrm{f}^c)^2} \sqrt{\sum_{\mathrm{x}=1}^{n} (\mathrm{f}^d)^2}} \tag{30}$$

Chromosome sequencing of image pixel distances provides 90% accurate grouping. Their technique examines the contrast between two sets of images.

Here $||\mathrm{a}, \mathrm{b}||_{\mathrm{e}}$ denotes the normal distance value of genetic pixel image, $\mathrm{C}_{\mathrm{min}}$ implies selected feature vector, $||\mathrm{a}, \mathrm{b}||_{\mathrm{e}}$ lies the minimum distance from f^d. The DVSNN model is designed to handle and process complex visual data, including images with limited quality or information. By utilizing a deep neural network architecture, the DVSNN learns intricate patterns and features from the data, enabling it to classify and predict the risk of genetic disorder based chromosomal abnormalities even in the presence of noisy or low-quality image inputs. This aspect of the proposed methodology ensures robust performance in scenarios where data quality is a challenge.

3.5.3 Chromosome Abnormality detection

After classification, the following stage is fetal genetic disorder detection and analysis. The contribution to this stage is the sequencing of chromosomes from vectorized versatile measurements.

Table 2 Collected test cases with their types

Case type	No. of cases
Normal (N)	5
Trisomy 13 Type (Patau Syndrome)	5
Trisomy 18 Type (Edwards Syndrome)	5
Monosomy X Type (Turner Syndrome)	4

Table 1 shows the case type and cases; the collected experimental intervals include different natural and numerical values. Conclusions are made based on chromosome number and conventional condition reports.

Count the total number of diverse metaphase chromosomes detected and the number of chromosomes for each predicted class (13, 18, and X). Trisomy 13 (Badau syndrome) is diagnosed when the entire number of chromosomes reaches 47, including 3 chromosomes 13.

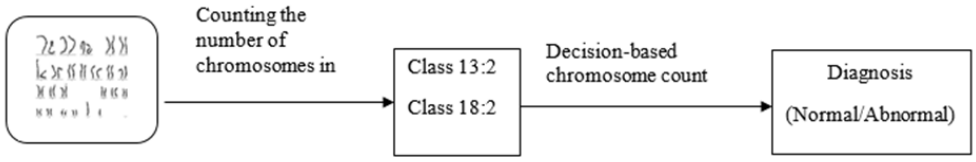

Fig. 8 Abnormality Detection

Figure 8 shows the final step, which is genetic-based chromosome abnormalities detection using the proposed classifier. The altered chromosome is the input, and the diagnosis is the output.

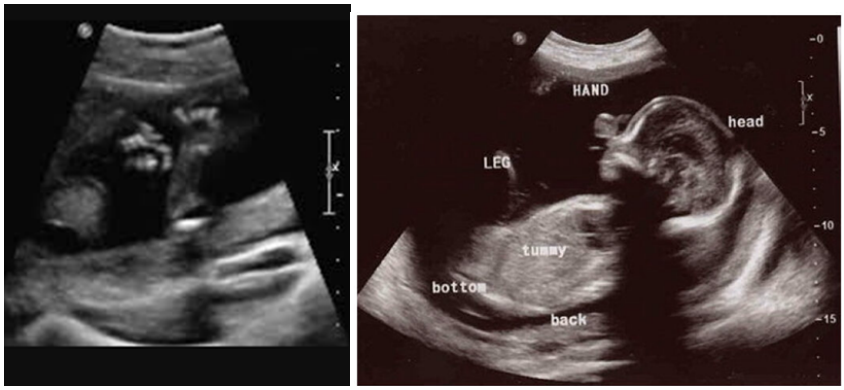

Fig. 9 Trisomy 18 ultrasound images

The next most prevalent autosomal trisomy in neonates is trisomy 18 (Edwards's syndrome). The mother's nondisjunction of chromosome 18 accounts for more than 90% of cases. Prenatal ultrasound may identify the distinct anatomical abnormalities present in fetuses with trisomy 18. Abnormalities in the face, hands, and limbs are classified as mild abnormalities in Figure 9.

$$CA = \frac{\sum_{i=1}^{m}(v_x - \bar{v})(u_x - \bar{u})}{\sum_{x=1}^{x=1}[(v_x - \bar{v})^2]^{1/2} \sum_{x=1}^{x=m}[(v_x - \bar{v})^2]^{1/2}} \tag{31}$$

This DVSNN calculates the correlation coefficient between the detected matching candidates with chromosome abnormalities.
$\sum_{x=1}^{x=1}[(v_x - \bar{v})^2]^{1/2} \sum_{x=1}^{x=m}[(v_x - \bar{v})^2]^{1/2}-$ The grey values of x^th pixel of images, m total number of pixels within the images.

Genetic chromosomal aberrations usually result from mistakes or damage during cell division. Chromosomal abnormalities are caused by excess or missing chromosomes detecting the abnormalities and improving the accuracy.

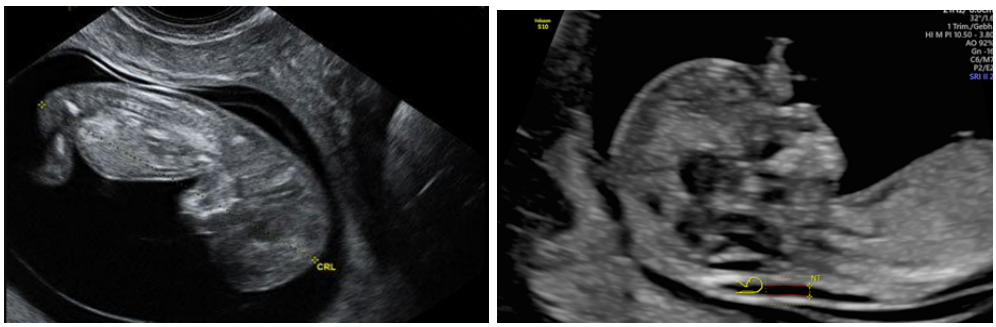

Fig. 10 Trisomy (21) Down Syndrome

Chromosome 21 at conception (47, XX, +21 or 47, XY, +21) account for approximately 95% of cases of karyotypic abnormalities. Chromosomes 14 and 21 are often involved in trisomy 21 translocations, which occur in 2% of cases and are usually familial. Figure 10 shows the sample of trisomy (21) Down syndrome images.

4 Result and discussion

This division executed the proposed system in Python using the Anaconda tool on the Deep Learning libraries. Processor: Intel(R) Core(MT) i7 @ 4.00GHz, and 8 GB RAM. In the proposed DVSNN method is compared with a CNN, DCNN and a U-Net Algorithm for chromosome abnormality detection.

Table 3 Proposed method Simulation parameters

Parameters	Values
Name of the Dataset	Cytogenetic Service Unit dataset
Tool	Anaconda
Language	Python
Total count of Images	1000
Training images (70%)	700
Testing images (30%)	300

Table 2 describes Cytogenetic service unit data set for testing the performance of the proposed system. Classification has been evaluated on both the training and test datasets.

- True Positive (TP): Image is correctly classified into positive (p) class.
- False Positive (FP): An image is incorrectly classified as positive (p).
- False Negative (FN): An image has been misclassified as a negative (N) class.
- True Negatives (TN): The image is properly classified as a negative class (N).

Table 4 Precision performance Analysis

Number of images / Classification methods	CNN in %	DCNN in %	U-Net in %	DVSNN in %
50	47	51	59	72
100	55	62	69	76
150	65	78	80	84
200	71	77	79	86
250	78	82	86	89
300	82	86	91	94

4.1 Comparison performance

Table 3 shows the proper accurateness's (also called positive classes) as a percentage of the corresponding occurrences. For a two-class asymmetric classification problem, accuracy is divided by the number of true positives and false positives.

$$Precision\,(P) = \sum TP/\left(\sum TP + \sum FP\right) * 100 \tag{32}$$

Here, TP denotes the true positive and FP lies the false positives.

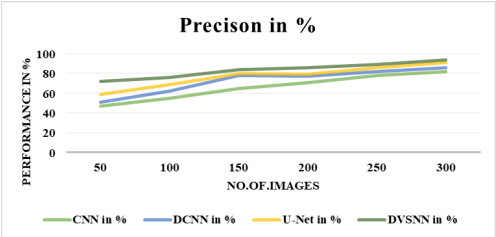

Fig. 11 Result of precision analysis

Figure 11 shows the accuracy of the TP values used to compare the different methods. The proposed implementation offers higher performance than other algorithms. Of the existing methods, CNN accounts for 80%, DCNN accounts for 86%, and U-Net accounts for 91%. Nevertheless, the proposed method, using DVSNN, showed 300 images with 94% higher accuracy than the previous method.

Figure 12 shows the sensitivity performance for detecting fetus genetic disorder chromosomal abnormalities. This is because can see how many positive examples the model identified correctly. The sensitivities of the existing methods are CNN 80%, DCNN 84%, and U-Net 90%; however, the proposed DVSNN method in this paper achieved a sensitivity of 91% than the traditional method using 300 images.

Table 4 shows that the TP recall diverged due to the total number of features belonging to the positive genetic disorder category, as shown in the equation below.

$$Recall(R) = \Sigma TP/(\Sigma TP + \Sigma FN) * 100 \tag{33}$$

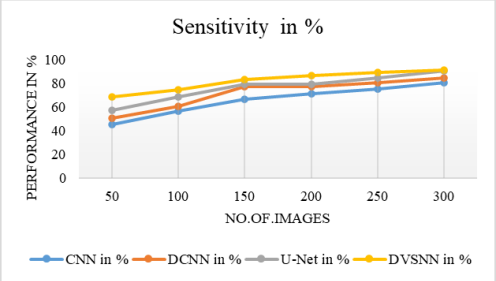

Fig. 12 Sensitivity Performance

Table 5 Recall performance

Number of images	CNN in %	DCNN in %	U-Net in %	DVSNN in %
50	40	51	55	67
100	49	58	60	70
150	60	72	75	79
200	74	79	82	84
250	79	81	85	89
300	86	88	90	92

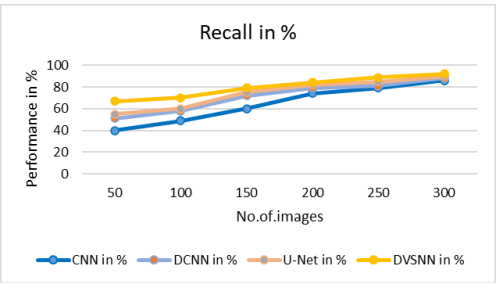

Fig. 13 Analysis of recall performance

Figure 13 compares the recall performance for detecting fetus genetic chromosomal abnormalities. The proposed implementation provides better performance than the other methods. In the previous method, CNN was 86%, DCNN 88%, and U-NET 90% for 300 images.

Figure 14 shows the sensitivity performance for detecting chromosomal abnormalities in fetal genetic disorders. Existing methods achieve 78% accuracy for CNN, 82% accuracy for DCNN, and 89% accuracy for U-Net, but the proposed DVSNN method reaches 90% accuracy, which is more than the traditional method using 300 images.

Table 5 describes the different stages of user generation to enable accurate chromosomal aberration detection. Compared to various methods, the proposed system significantly influences accuracy performance.

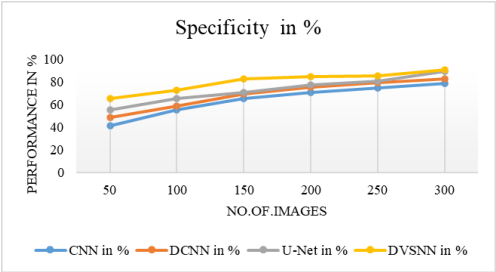

Fig. 14 Result of specificity performance analysis

Table 6 Impact of Accuracy

Number of images	CNN in %	DCNN in %	U-Net in %	DVSNN in %
50	55	58	61	68
100	59	60	70	75
150	69	76	80	85
200	77	82	85	90
250	79	84	91	93
300	84	88	90	96

$$Accuracy\,(A) = \Sigma TP/\left(\Sigma TP + \Sigma TN\right) * 100 \tag{34}$$

Here, TN lies the true negative.

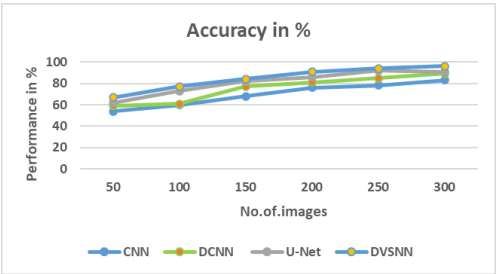

Fig. 15 Analysis of accuracy for genetic disorder chromosomal abnormalities detection

Figure 15 shows the accuracy of identifying chromosomal abnormalities in genetic diseases. The proposed implementation is more accurate than the other methods. The accuracies of the conventional methods are 83% for CNN, 89% for DCNN, and 91% for U-NET, all of which are higher than traditional methods.

Figure 16 describes the training and testing accuracy performance for detecting fetus genetic disorder chromosomal abnormalities. In each epoch of training and testing, the proposed DVSNN model improved the accuracy of detecting chromosomal abnormality. The system's improved anomaly detection capability is reflected by lower loss values.

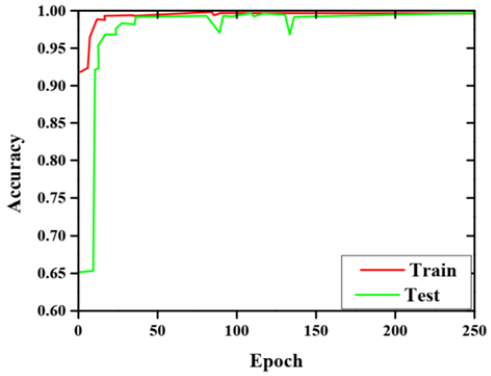

Fig. 16 Accuracy model

Table 7 False score

Number of images	CNN in %	DCNN in %	U-Net in %	DVSNN in %
50	35	33.3	32.1	27.4
100	45.2	40.2	38.8	29.5
150	47.1	43.5	42.3	30.5
200	55.2	50.8	49.5	38.5
250	59.4	52.8	50.7	44.8
300	60.2	57.5	52.8	50.7

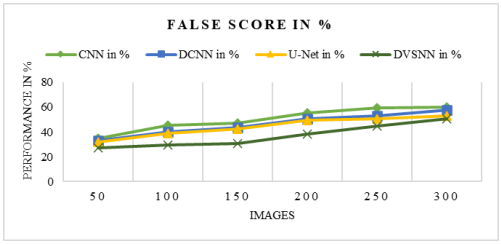

Fig. 17 Analysis of False Rate

Table 6 describes the false rate and compares the chromosome features at different levels for error reduction. This method minimizes the errors of the images in both the training and testing images.

Figure 17 describes False Rate (FR) values for looking at changed techniques, the proposed execution reduces the error of contrasting different methods. CNN) is 60.2%, DCNN is 57.5 and U-net is 52.8% but the proposed DVSNN method is 50.7%.

Table 7 shows that each of the 150 positive cases and 150 negative cases had multiple metaphases that could be analyzed metaphases were detected in each of the 150 positive cases and 4 negative cases in the table in abnormal cells. Based on the

Table 8 Normal and abnormal class

Methods 2-5	Normal class-150		Abnormal class-150	
	Correct	Incorrect	Correct	Incorrect
DVSNN	100	50	150	0
CNN	95	45	80	50
DCNN	140	10	120	30
U-net	80	70	75	65

pre-established classification rules, 150 positive cases and 0 negative cases were found in the test database.

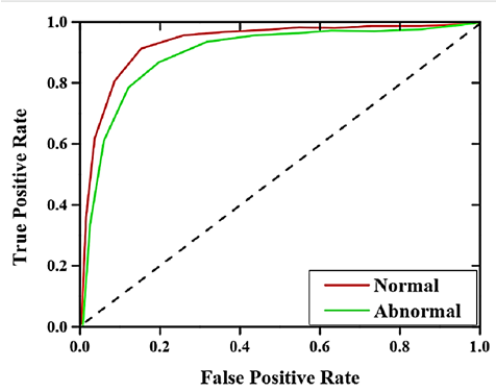

Fig. 18 Normal and Abnormal Curve Analysis

Figure 18 demonstrates the normal and abnormal curves for the cytogenetics dataset. The DVSNN model was developed using this dataset to identify chromosomal abnormalities. Its performance is in anomaly detection, and the proposed DVSNN algorithm outperforms other algorithms on the karyotype image dataset. The DVSNN model achieved the highest efficiency percentage of 98.2% on the Cytogenic Service Unit dataset.

5 Conclusion

Recently, there has been an increasing demand for automated systems to detect abnormalities to assist cytogenetic and save valuable time. In this paper, we propose a method for identifying and classifying individual chromosomes using deep learning techniques. Classification level DVSNN uses transfer learning to detect chromosomal abnormalities in genetic diseases. Pre-trained models Feature extraction and classification using datasets from biomedical imaging laboratories surpass state-of-the-art techniques. It is found that the classification accuracy of all the experimental CEGMR datasets is very high with an accuracy rate of 96%. The DVSNN is fine-tuned by combining each convolutional layer with a block normalization layer in the element extraction domain and replacing the top representation layer (fully correlated layer)

with a global mean pooling layer. Increasing the amount of training can improve the accuracy so that future work will increase the number of intermediate images in the dataset.

Conflict of Interest Statement. The authors declare that the research was conducted in the absence of any commercial or financial relationships that could be construed as a potential conflict of interest.

Author Contributions. S.P. (Srinivasan P): Conceptualization of the study, methodology design (ISCS + DVSNN framework), implementation of algorithms, and drafting of the manuscript.

R.S.S. (Sabeenian R.S.): Supervision, validation of experimental results, critical review, and editing of the manuscript.

References

[1] Tang J, Han J, Jiang Y, Xue J, Zhou H, Hu L, Chen C, Lu L. An Innovative Three-Stage Model for Prenatal Genetic Disorder Detection Based on Region-of-Interest in Fetal Ultrasound. Bioengineering. 2023; 10(7):873. https://doi.org/10.3390/bioengineering10070873.

[2] Tang J, Han J, Xue J, Zhen L, Yang X, Pan M, Hu L, Li R, Jiang Y, Zhang Y, Jing X, Li F, Chen G, Zhang K, Zhu F, Liao C, Lu L. A Deep-Learning-Based Method Can Detect Both Common and Rare Genetic Disorders in Fetal Ultrasound. Biomedicines. 2023 Jun 19;11(6):1756. doi: 10.3390/biomedicines11061756.

[3] Elavarasi T, Mariappan P "A DEEP LEARNING APPROACH TO DETECT GENETIC BASED DISEASE IN PREGNANCY PERIOD", International Research Journal of Engineering and Technology (IRJET), Volume: 11 Issue: 11 — Nov 2024, pp. 311-316.

[4] Q. Zhao, G. Yao, F. Akhtar, J. Li and Y. Pei, "An Automated Approach to Diagnose Turner Syndrome Using Ensemble Learning Methods," in IEEE Access, vol. 8, pp. 223335-223345, 2020, doi: 10.1109/ACCESS.2020.3039867.

[5] W. Ding, L. Chang, C. Gu, and K. Wu, "Classification of chromosome karyotype based on faster-run with the segmentation and enhancement pre-processing model," in 2019 12th International Congress on Image and Signal Processing, BioMedical Engineering and Informatics (CISPBMEI). IEEE, 2019, pp. 1–5.

[6] Y. Qin, J. Wen, H. Zheng, X. Huang, J. Yang, N. Song, Y.-M. Zhu, L. Wu, and G.-Z. Yang, "Varifocal-net: A chromosome classification approach using deep convolutional networks," IEEE transactions on medical imaging, vol. 38, no. 11, pp. 2569–2581, 2019.

[7] W. Zhang, S. Song, T. Bai, Y. Zhao, F. Ma, J. Su, and L. Yu, "Chromosome classification with convolutional neural network based deep learning," in 2018 11th International Congress on Image and Signal Processing, BioMedical Engineering and Informatics (CISP-BMEI). IEEE, 2018, pp. 1–5.

[8] Vinya Vijayan; Remya R S;Sabeena K "Survey On Chromosome Image Analysis For Abnormality Detection In Leukemias" International Journal of Research in Engineering and Technology , Vol 04, Issue: 04 ,April 2015 .

[9] Revathy M Nair, Remya R S, Sabeena K "Karyotyping Techniques of Chromosomes: A Survey" International Journal of Computer Trends and Technology (IJCTT) ,Vol 22, Number 1,April 2015.

[10] W. Ding, L. Chang, C. Gu, and K. Wu, "Classification of chromosome karyotype based on faster-rcnn with the segmatation and enhancement pre-processing model," in 2019 12th International Congress on Image and Signal Processing, BioMedical Engineering and Informatics (CISPBMEI). IEEE, 2019, pp. 1–5.

[11] W. Zhang, S. Song, T. Bai, Y. Zhao, F. Ma, J. Su, et al., "Chromosome classification with convolutional neural network based deep learning", 2018 11th International Congress on Image and Signal Processing BioMedical Engineering and Informatics (CISP-BMEI), pp. 1-5, 2018.

[12] W. Ding, L. Chang, C. Gu and K. Wu, "Classification of chromosome karyotype based on faster-rcnn with the segmatation and enhancement pre-processing model", 2019 12th International Congress on Image and Signal Processing BioMedical Engineering and Informatics (CISPBMEI), pp. 1-5, 2019.

[13] Y. Qin, J. Wen, H. Zheng, X. Huang, J. Yang, N. Song, et al., "Varifocal-net: A chromosome classification approach using deep convolution networks", IEEE transactions on medical imaging, vol. 38, no. 11, pp. 2569-2581, 2019.

[14] T. L. Ryan et al., "Optimization and validation of automated dicentric chromosome analysis for radiological/nuclear triage applications", Mutat Res Gen Tox En, 847, (2019)

[15] J. Bi et al., "Rapid and High-Throughput Detection of Peripheral Blood Chromosome Aberrations in Radiation Workers", International Dose-Response Society, 17, 2 (2019)

[16] J. Liu et al., "Accurate cytogenetic biodosimetry through automated dicentric chromosome curation and metaphase cell selection", F1000Research. 6, 1396 (2017)

[17] X. Shen et al., "A dicentric chromosome identification method based on clustering and watershed algorithm", Scientific Reports, 9, 2285 (2019)

[18] M. S. Al-Kharraz, L. A. Elrefaei and M. A. Fadel, "Automated System for Chromosome Karyotyping to Recognize the Most Common Numerical Abnormalities Using Deep Learning," in IEEE Access, vol. 8, pp. 157727-157747, 2020, doi: 10.1109/ACCESS.2020.3019937.

[19] F. Abid and L. Hamami, "A survey of neural network based automated systems for human chromosome classification," Artif. Intell. Rev., vol. 49, no. 1, pp. 41–56, Jan. 2018.

[20] R. Hu, J. Karnowski, R. Fadely, and J.-P. Pommier, "Image segmentation to distinguish between overlapping human chromosomes," CoRR, vol. abs/1712.07639, 2017. [Online]. Available: http://arxiv.org/abs/ 1712.07639.

[21] H. M. Saleh, N. H. Saad, and N. A. M. Isa, "Overlapping chromosome segmentation using U-net: Convolutional networks with test time augmentation," Procedia Comput. Sci., vol. 159, pp. 524–533, 2019.

[22] A. O. Kusakci, B. Ayvaz, and E. Karakaya, "Towards an autonomous human chromosome classification system using competitive support vector machines teams (CSVMT)," Expert Syst. Appl., vol. 86, pp. 224–234, Nov. 2017.

[23] D. Somasundaram, "Structural similarity and probabilistic neural network based human G-band chromosomes classification," Int. J. Hum. Genet., vol. 18, no. 3, pp. 228–237, Apr. 2018.

[24] W. Zhang, S. Song, T. Bai, Y. Zhao, F. Ma, J. Su, and L. Yu, "Chromosome classification with convolutional neural network based deep learning," in Proc. 11th Int. Congr. Image Signal Process., Biomed. Eng. Informat. (CISP-BMEI), Oct. 2018, pp. 1–5.

[25] D. Somasundaram, "Machine learning approach for homolog chromosome classification," Int. J. Imag. Syst. Technol., vol. 29, no. 2, pp. 161–167, Jun. 2019.

[26] R. Huang et al., "A clinical dataset and various baselines for chromosome instance segmentation", IEEE/ACM Transactions on Computational Biology and Bioinformatics, vol. 19, no. 1, pp. 31-39, 2021.

[27] W. Ding, L. Chang, C. Gu and K. Wu, "Classification of chromosome karyotype based on faster-rcnn with the segmatation and enhancement pre-processing model", 2019 12th International Congress on Image and Signal Processing BioMedical Engineering and Informatics (CISP-BMEI), pp. 1-5, 2019.

[28] X. Hu et al., "Classification of metaphase chromosomes using deep convolutional neural network", Journal of Computational Biology, vol. 26, no. 5, pp. 473-484, 2019.

[29] L. Xiao et al., "DeepACEv2: Automated chromosome enumeration in metaphase cell images using deep convolutional neural networks", IEEE Transactions on Medical Imaging, vol. 39, no. 12, pp. 3920-3932, 2020.

[30] N Nimitha, C Arun, AS Puvaneswari, B Paninila, VP Pavithra and B Pavithra, "Literature survey of chromosomes classification and anomaly detection using machine learning algorithms", Published under licence by IOP Publishing Ltd IOP Conference Series: Materials Science and Engineering Volume 402 2nd International conference on Advances in Mechanical Engineering (ICAME 2018), 22–24 March 2018.

[31] N. Madian, K. Jayanthi and S. Suresh, "Analysis of human chromosome images: Application towards an automated chromosome classification", International Journal of Imaging Systems and Technology, vol. 28, no. 4, pp. 235-245, 2018.

[32] H. Park, S.-M. Chun, J. Shim, J.-H. Oh, E. J. Cho, H. S. Hwang, J.-Y. Lee, D. Kim, S. J. Jang, S. J. Nam et al., "Detection of chromosome structural variation by targeted next-generation sequencing and a deep learning application", Scientific reports, vol. 9, no. 1, pp. 3644, 2019.

[33] A. S. Balajee et al., "Development of electronic training and telescoring tools to increase the surge capacity of dicentric chromosome scorers for radiological/nuclear mass casualty incidents", Applied Radiation and Isotopes 144, 111-117 (2019).

[34] Murugappan, V., & Sabeenian, R. S. (2017). Texture based medical image classification by using multi-scale gabor rotation-invariant local binary pattern (MGRLBP). Cluster Computing, 22(S5), 10979–10992. https://doi.org/10.1007/s10586-017-1269-6.

[35] Arunachalam, M., & Sabeenian,R.S (2018a). A novel prognosis and segmentation of necrosis (dead cells) in contrast enhanced T1-weighted glioblastoma tumor with automatic contextual clustering. International Journal of Imaging Systems and Technology, 29(1), 65–76. https://doi.org/10.1002/ima.22295

[36] Manju ,K., & Sabeenian, R. S. (2019). Cup and Disc Ratio and Inferior, Superior, Temporal and Nasal Calculation for Glaucoma Identification. Journal of Medical Imaging and Health Informatics, 9(6), 1316–1319. https://doi.org/10.1166/jmihi.2019.2720

[37] Sabeenian, R. S. & Kavitha, K.R., (2020). Long term monitoring of sleep disordered breathing using IOT enabled polymer sensor embedded fabrics. International Journal of Psychosocial Rehabilitation, 24(5), 7093–7101. https://doi.org/10.37200/ijpr/v24i5/pr2020718

[38] Kasinathan, P., Prabha, R., Sabeenian, R. S., Baskar, K., Ramkumar, A., & Mamo, S. A. (2022). Development of Deep Learning Technique of Features

for the Analysis of Clinical Images Integrated with CANN. BioMed Research International, 2022, 1–7. https://doi.org/10.1155/2022/2742274

[39] Thiyaneswaran, B., Sengottaiyan, K., Kulandairaj, M. S., & Dang, H. (2022). An effective model for the iris regional characteristics and classification using deep learning alex network. Iet Image Processing, 17(1), 227–238. https://doi.org/10.1049/ipr2.12630

[40] Thiyaneswaran, B., Anguraj, K., Kumarganesh, S., & Thangaraj, K. (2020). Early detection of melanoma images using gray level co-occurrence matrix features and machine learning techniques for effective clinical diagnosis. International Journal of Imaging Systems and Technology, 31(2), 682–694. https://doi.org/10.1002/ima.22514

[41] D. Sandhiya and B. Thiyaneswaran, "Extraction of dorsal palm basilic and cephalic hand vein features for human authentication system," 2017 International Conference on Wireless Communications, Signal Processing and Networking (WiSPNET), Chennai, India, 2017, pp. 2231-2235, doi: 10.1109/WiSPNET.2017.8300156.

[42] B. Thiyaneswaran, A. Saravanakumar and R. Kandiban, "Extraction of mole from eye sclera using object area detection algorithm," 2016 International Conference on Wireless Communications, Signal Processing and Networking (WiSPNET), Chennai, India, 2016, pp. 1413-1417, doi: 10.1109/WiSPNET.2016.7566369.

[43] K Jayasakthi velmurugan, P Srinivasan, A Gayathri, S Yuvarani"Melanoma Boundaries Detection Techniques Using Artificial Intelligence",3rd International conference on Artificial intelligence and smart energy(ICAIS 2023), ISBN 978-1-6654-6215.

[44] Bhartiya, S., Pushpakumar, R., Srinivasan, P., Aparna, N., Karthika, K., & Chauhan, A. (2023). Image analysis of MRI-based brain tumor classification and segmentation using BSA and RELM networks. 2023 2nd International Conference on Automation, Computing and Renewable Systems (ICACRS). https://doi.org/10.1109/icacrs58579.2023.10405052.

[45] Saranya Sekar, Lakshmi Sankaran, An efficient genetic disorder detection framework using adaptive segmentation and classification mechanism from chromosome images, Expert Systems with Applications, Volume 279, 2025, 127303, ISSN 0957-4174, https://doi.org/10.1016/j.eswa.2025.127303.

[46] Tabassum, S., Khan, M. J., Iqbal, J., Waris, A., & Ijaz, M. A. (2025). Automated karyogram analysis for early detection of genetic and neurodegenerative disorders: A hybrid machine learning approach. Frontiers in Computational Neuroscience, 18, 1525895. https://doi.org/10.3389/fncom.2024.1525895.

[47] Nimitha, N., Ezhumalai, P., & Chokkalingam, A. Chromosome Abnormality Detection Using Visual Geometric Transformer and Mantis Search Optimization. Microscopy Research and Technique. https://doi.org/10.1002/jemt.70026.

[48] C. -E. Kuo, J. -Z. Li, J. -J. Tseng, F. -C. Lo, M. -J. Chen and C. -H. Lu, "ChromosomeNet: Deep Learning-Based Automated Chromosome Detection in Metaphase Cell Images," in IEEE Open Journal of Engineering in Medicine and Biology, vol. 6, pp. 227-236, 2025, doi: 10.1109/OJEMB.2024.3512932.

[49] Mohammed El Amine Bechar, Jean-Marie Guyader, Marwa El Bouz, Nathalie Douet-Guilbert, Ayman Al Falou, Marie-Bérengère Troadec, Highly Performing Automatic Detection of Structural Chromosomal Abnormalities Using Siamese Architecture, Journal of Molecular Biology, Volume 435, Issue 8, 2023,168045,ISSN 0022-2836, https://doi.org/10.1016/j.jmb.2023.168045.

[50] Anitha, A (2024), "Ultrasound Fetus Dataset", Mendeley Data, V1, doi: 10.17632/yrzzw9m6kk.1.